Thermal and Electrical Characterization of Silicon and Germanium Transistors Using I–V Measurements

Peter Khorani

PHY 353L Modern Laboratory
Department of Physics
The University of Texas at Austin
Austin, TX 78712, USA

December 2, 2025

Abstract

This experiment investigated temperature-dependent carrier transport in bipolar junction transistors by measuring forward-bias I–V characteristics of silicon (Si) and germanium (Ge) NPN devices. The base–emitter junctions were driven by a programmable NI DAQ, the collector currents were measured with a Keithley 6485 picoammeter, and the devices were mounted on a heated aluminum plate monitored by a type-K thermocouple. For silicon, semilogarithmic I–V curves exhibited a clear exponential region consistent with the Shockley equation; fits to $\ln I_C$ versus V_{BE} yielded ideality factors $n_{\mathrm{Si}} \approx 1.0$ and saturation currents $I_s(T)$ that increased strongly with temperature. An Arrhenius analysis of $I_s(T)$ gave an effective band gap $E_g^{(\mathrm{Si})} \approx 1.2 \pm 0.3$ eV, in reasonable agreement with the accepted 1.12 eV value. In contrast, the Ge device showed substantial leakage and early series-resistance effects: wide ± 1.3 V fits produced nonphysical parameters, while restricted low-bias "small-window" fits over $0.01 \leq V_{BE} \leq 0.10$ V yielded more reasonable $n_{\mathrm{Ge}} \approx 0.7$–$1.1$ but did not support a reliable band-gap estimate. Overall, the silicon results confirm the Ebers–Moll/ Shockley description of the base–emitter junction, whereas the germanium data highlight the need to choose an operating regime in which the model assumptions are actually satisfied when extracting semiconductor parameters from transistor I–V curves.

1 Introduction

1.1 Motivation

Semiconductors form the basis of nearly all modern electronics, from discrete diodes and transistors to integrated circuits containing billions of devices. The electronic transport properties of semiconductors arise from the thermal occupation of bands separated by an energy gap, the magnitude of which governs the density of thermally excited carriers and therefore the conductivity of the material [3]. Because the carrier density depends exponentially on the ratio E_g/kT, even modest temperature changes significantly alter a semiconductor's electrical behavior.

A bipolar junction transistor (BJT), in which a thin p-type region is sandwiched between two n-type regions, relies on this strong sensitivity of carrier populations to voltage and temperature. When biased in forward-active mode, its base–emitter junction behaves as a diode whose current–voltage relationship reflects the underlying carrier transport physics [2]. By measuring this forward-bias characteristic over a controlled temperature range, one can extract both device-level parameters such as the *ideality factor* n and material properties such as the effective *band gap* E_g.

Thus, the present experiment has two primary goals: (i) to investigate the exponential dependence of the collector current on base–emitter voltage and temperature, and (ii) to test the Ebers–Moll model by extracting n, $I_s(T)$, and E_g for both silicon and germanium. This provides a direct experimental demonstration of semiconductor carrier statistics.

1.2 Theoretical Background

Band structure and thermal excitation In crystalline semiconductors, electrons occupy Bloch states in a valence band and a conduction band separated by a band gap E_g . At finite temperature, the occupation probability of a state of energy E is given by the Fermi–Dirac distribution. For non-degenerate semiconductors, this reduces to a Boltzmann expression, such that the population of conduction-band electrons scales approximately as

$$n \propto T^{3/2} \exp\left(-\frac{E_g}{2kT}\right). \tag{1}$$

This strong temperature dependence ultimately governs the saturation current in a diode or transistor.

Ebers–Moll equation and ideality factor The base-emitter junction of an NPN transistor obeys the Shockley diode equation, derived from the Ebers-Moll model:

$$I_C = I_s \left(e^{qV_{BE}/(nkT)} - 1 \right), \tag{2}$$

where I_s is the saturation current and n is the ideality factor. For an ideal diffusion-dominated junction, $n \approx 1$, whereas values $n > 1$ indicate recombination-dominated or series-resistance limited transport [1]. In the forward-bias regime where $qV_{BE} \gg nkT$, Eq. (2) simplifies to

$$I_C \approx I_s e^{qV_{BE}/(nkT)}. \tag{3}$$

Therefore,

$$\ln I_C = \ln I_s + \frac{q}{nkT} V_{BE}, \tag{4}$$

so a semilogarithmic plot of $\ln I_C$ versus V_{BE} should produce a straight line in the ideal transport region.

Temperature dependence of saturation current and band gap The saturation current I_s depends sensitively on the density of thermally excited minority carriers. A widely used approximation for its temperature dependence is [1]:

$$I_s(T) \propto T^3 \exp\left(-\frac{E_g}{kT} \right). \tag{5}$$

Equation (5) can be rearranged into an Arrhenius form,

$$\ln\left(\frac{I_s}{T^3} \right) = -\frac{E_g}{k} \frac{1}{T} + \text{const}, \tag{6}$$

so that a plot of $\ln(I_s/T^3)$ versus $1/T$ yields a straight line. The slope of this line directly gives the band gap E_g.

At room temperature, germanium has a significantly smaller band gap ($E_g^{(\mathrm{Ge})} \approx 0.66$ eV) than silicon ($E_g^{(\mathrm{Si})} \approx 1.12$ eV) [3]. As a result, one should expect germanium to exhibit larger leakage currents, stronger temperature dependence, and more pronounced deviation from ideality.

1.3 Our Experimental Approach

In this experiment, we treat the base–emitter junction of both silicon and germanium BJTs as effective diodes and measure their forward-bias I–V characteristics over a wide range of temperatures. A National Instruments

(NI) data acquisition system provides a programmable base–emitter voltage, allowing submillivolt control and fine-resolution voltage sweeps. The collector is biased through an accurately measured series resistor (0.995 kΩ for Si and 0.997 kΩ for Ge), and the resulting collector current is measured using a Keithley 6485 picoammeter. The transistor packages are thermally anchored to an aluminum plate containing a 71 Ω, 25 W power resistor used as a controllable heater. A type-K thermocouple, read by the DAQ, monitors the temperature of the plate.

At each temperature point, we record a complete forward-bias I–V curve for both materials. We then identify the linear regions of $\ln I_C$ versus V_{BE}, extract n and I_s, and use Eq. (6) to obtain the effective band gaps. Comparing silicon and germanium allows us to test the predictions of band theory, the Shockley diode model, and the temperature dependence of minority carriers.

2 Experimental Setup

2.1 Apparatus

The electrical and thermal characterization of the silicon (Si) and germanium (Ge) transistors was performed using a combination of a programmable data acquisition system, precision current metering, and a thermally controlled mounting assembly. A schematic overview of the apparatus is shown in Fig. 1, and the essential instrumentation is summarized below.

Transistor Samples. The semiconductor devices studied were discrete NPN bipolar junction transistors, one fabricated in silicon and the other in germanium. The silicon package was a model TIP29C transistor, from which one could pull the manual; however, the germanium package is an unknown model. Each transistor package was mounted against an aluminum plate to ensure uniform thermal contact. The collector and base terminals were externally accessible through labeled binding posts, while the emitter was routed through a shielded BNC connection to the picoammeter input.

Collector Bias Network. A dedicated low-voltage bench supply provided the collector bias. Its positive terminal was connected to the transistor collector through a precisely measured series resistor:

$$R_{C,\mathrm{Si}} = (0.995 \pm 0.005)\,\mathrm{k}\Omega, \qquad R_{C,\mathrm{Ge}} = (0.997 \pm 0.005)\,\mathrm{k}\Omega,$$

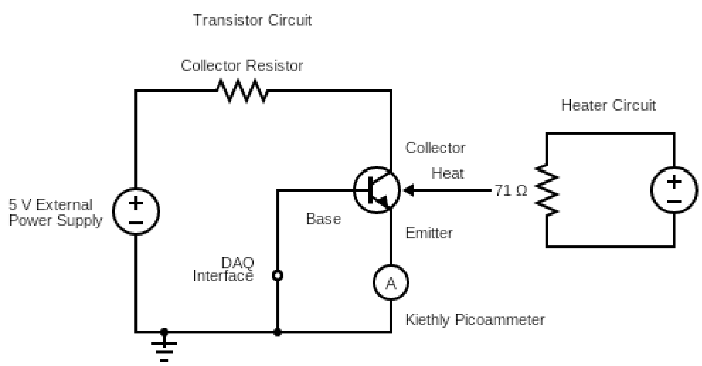

Figure 1: Circuit used to bias the transistor and measure its I–V characteristics. The collector is biased from a low-voltage supply through a measured resistor $R_C \approx 1$ kΩ, while the base–emitter junction is driven by an effective source V_{BE}. The emitter current I_C is measured by a picoammeter placed in series with the emitter. A separate isolated supply drives the 71 Ω heater resistor clamped to the mounting plate.

determined using a 4-wire ohmic measurement. The negative terminal of this supply defined the global circuit ground G, which served as the reference for all analog signals. This arrangement ensures that the resulting collector current is set by the base–emitter drive and measured directly by the picoammeter.

Current Measurement: Keithley 6485. The collector current was measured using a Keithley 6485 picoammeter operating in DC current mode. The transistor emitter lead was connected to the `INPUT HI` terminal of the picoammeter via a BNC-to-banana adapter, while the `INPUT LO` terminal was tied to the common ground G. The meter's analog voltage output (proportional to the measured current with an inverting transfer function) was fed into an NI DAQ analog input channel (AI0), enabling synchronous digitization of current, voltage, and temperature. The low input burden voltage of the 6485 ensured that the emitter remained close to ground potential, allowing accurate programming of the base–emitter voltage.

Base Drive: NI Data Acquisition System. Programmable forward-bias voltages for the base–emitter junction were supplied using the analog

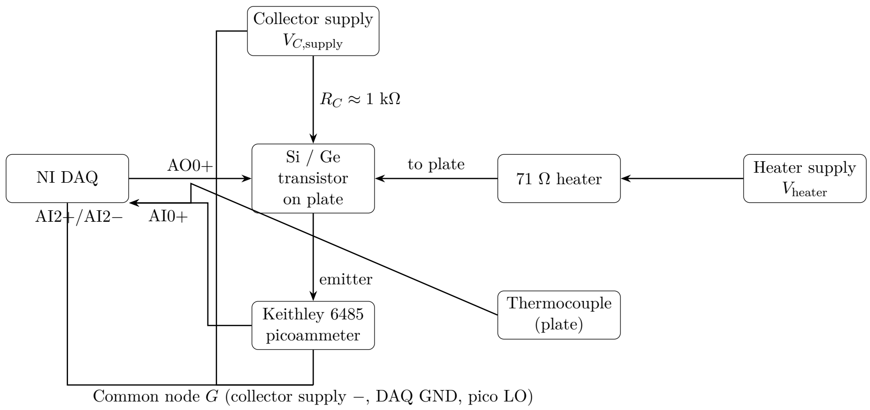

Figure 2: Block diagram of the measurement setup. The NI DAQ drives the base–emitter voltage via AO0 and reads the collector current from the Keithley 6485 on AI0. The collector is biased from a separate low-voltage supply through a measured $R_C \approx 1$ kΩ. A second isolated supply powers the 71 Ω heater attached to the aluminum plate, whose temperature is monitored by a thermocouple read on AI2. All measurement electronics share a common ground node G, while the heater supply remains electrically isolated.

output channel AO0 of a National Instruments DAQ. The AO0 high terminal was connected directly to the transistor base (optionally through a base resistor), while the AO0 ground terminal was tied to the common node G. This configuration allowed fine-grained voltage sweeps across the junction, enabling measurement of currents spanning nine decades, from nanoamps to tens of milliamps. By digitizing the picoammeter's output simultaneously, the DAQ provided synchronized (V_{BE}, I_C) measurements at each temperature.

Thermal Control and Temperature Measurement. To vary the device temperature, a 71 Ω, 25 W power resistor was firmly clamped to the same aluminum plate as the transistors. A second isolated bench supply drove this heater, with heater + and − forming a floating loop intentionally disconnected from G to avoid ground loops or parasitic current paths. By adjusting the heater voltage between 0 and 23 V, plate temperatures ranging from ambient to approximately 75°C were obtained.

Temperature was monitored using a type-K thermocouple inserted into a machined well beneath the transistor mounting position. Thermocouple leads were connected to DAQ differential channel AI2, and the temperature was computed using the DAQ's built-in cold-junction compensation and the NIST reference tables [4].

Data Acquisition Software. A custom LabVIEW VI controlled the voltage sweeps, acquired picoammeter output, measured the thermocouple voltage, and logged the complete dataset in tab-separated format for subsequent Python-based analysis. This ensured precise synchronization between voltage, current, and temperature measurements throughout each sweep.

The combined apparatus enabled full characterization of the forward-bias I–V behavior of Si and Ge transistors under controlled thermal conditions, allowing direct extraction of the ideality factor, saturation current, and temperature-dependent band-gap parameters.

2.2 Procedure

The measurement procedure consisted of three main stages: (i) wiring and verification of the electrical and thermal setup, (ii) establishing and stabilizing temperature setpoints, and (iii) automated acquisition of base–emitter I–V curves for both Si and Ge transistors at each temperature. In practice, we devoted additional time to resolving software and wiring issues for the first few lab periods, so the most extensive data sets were ultimately taken during the final lab sessions once the apparatus behaved reproducibly.

Electrical checkout and grounding. We first wired the circuit shown in Fig. 1 and the block diagram in Fig. 2. The collector supply positive terminal was connected to the transistor collector through the appropriate series resistor ($R_{C,\mathrm{Si}}$ or $R_{C,\mathrm{Ge}}$), while its negative terminal defined the global ground node G. The transistor emitter was routed to the `INPUT HI` terminal of the Keithley 6485 picoammeter; the `INPUT LO` terminal was tied directly to G, ensuring that the emitter potential remained close to ground. The picoammeter's analog voltage output was connected to NI DAQ channel AI0, and the DAQ ground (AO0−, AI0−, AI2−) was also tied to G, so that all measurement electronics shared a common reference.

The DAQ analog output AO0+ was wired to the transistor base to serve as the programmable base–emitter drive, with AO0− connected to G. With the heater supply disabled and the collector supply set to a modest voltage, we verified the wiring by stepping AO0 through a small range and observing (i) the corresponding change in V_{BE} with a handheld DMM and (ii) the proportional response of the picoammeter analog output on AI0. This step confirmed the sign convention, the approximate analog-output scaling factor of the picoammeter, and the absence of ground loops or obvious miswirings.

Temperature control and equilibration. After confirming the electrical chain, we mounted the Si and Ge transistors to the aluminum plate and clamped the 71 Ω heater resistor firmly against the same plate. The type-K thermocouple was inserted into its well beneath the mounting surface and connected in differential mode to DAQ channel AI2. With the heater supply still off, we recorded an initial room-temperature I–V sweep for each device to serve as a baseline and to verify that the plate, thermocouple, and transistor temperatures were initially in equilibrium.

To reach higher temperatures, we enabled the isolated heater supply and increased its output in steps, using four discrete heater voltages:

$$V_{\text{heater}} = 15,\ 17,\ 20,\ 23\ \text{V},$$

which produced approximate steady-state plate temperatures of

$$T \approx 38\text{–}40^{\circ}\text{C},\ 50\text{–}52^{\circ}\text{C},\ 60^{\circ}\text{C},\ 70\text{–}72^{\circ}\text{C},$$

respectively. After each change in heater voltage, we waited several minutes for the thermocouple reading to settle, monitoring the temperature trace in LabVIEW until the drift fell below a small threshold (of order a few tenths of a degree per minute). Once the temperature was stable, we recorded the thermocouple voltage and its corresponding temperature using the DAQ's built-in cold-junction compensation and the NIST type-K reference tables.[4]

Bias ranges and picoammeter settings at room temperature. At room temperature we carried out a systematic set of symmetric voltage sweeps around $V_{BE} = 0$ to probe both reverse leakage and forward conduction. For the silicon transistor we used three base–emitter ranges:

$$\begin{aligned} \text{Si:}\quad & -0.2\ \text{V} \le V_{BE} \le +0.2\ \text{V}, \\ & -0.4\ \text{V} \le V_{BE} \le +0.4\ \text{V}, \\ & -0.8\ \text{V} \le V_{BE} \le +0.8\ \text{V}. \end{aligned}$$

For the germanium transistor we repeated all of the above ranges and additionally extended the sweep to

$$\text{Ge:}\quad -1.3\ \text{V} \le V_{BE} \le +1.3\ \text{V},$$

in order to probe deeper into the high-current forward region.

For each sweep we selected the picoammeter full-scale range to balance dynamic range against resolution. At room temperature the silicon sweeps used:

$$\begin{aligned} -0.2 \text{ to } +0.2 \text{ V}: &\quad 200 \text{ nA full scale,} \\ -0.4 \text{ to } +0.4 \text{ V}: &\quad 20\ \mu\text{A full scale,} \\ -0.8 \text{ to } +0.8 \text{ V}: &\quad 20 \text{ mA full scale,} \end{aligned}$$

so that the low-bias sweeps emphasized small leakage currents and the largest sweep captured the onset of milliamp-level conduction. For the largest silicon and germanium ranges, $|V_{BE}| \leq 0.8$ V and $|V_{BE}| \leq 1.3$ V, the nominal full-scale setting was 20 mA to avoid saturating the meter at the highest forward currents. The germanium room-temperature sweeps used analogous settings, with the extended ± 1.3 V range again paired with the 20 mA scale.

Heated sweeps and time constraints. Because a significant fraction of the scheduled lab time was spent resolving software and wiring issues, the temperature-dependent measurements were taken under a tighter time constraint near the end of the experiment. For the heated silicon measurements, we prioritized coverage of all three voltage ranges but did not repeat the full matrix of conditions at every temperature. Specifically, we obtained:

- -0.2 V to $+0.2$ V sweeps at heater voltages 15 V and 23 V,
- -0.4 V to $+0.4$ V sweeps at 15 V and 23 V,
- -0.8 V to $+0.8$ V sweeps at all four heater voltages (15, 17, 20, 23 V).

For each of these heated silicon sweeps, the picoammeter full-scale settings were kept identical to the corresponding room-temperature ranges (200 nA, 20 μA, and 20 mA), so that the data could be compared directly without re-scaling the analog output.

For germanium at elevated temperatures, we concentrated on the most informative wide-bias sweeps. Due to the limited remaining time, we acquired only the -1.3 V to $+1.3$ V sweeps at each heater setting, rather than repeating the smaller ranges as at room temperature. However, we were able to confine all heated Ge sweeps to a 2 mA full-scale range on the picoammeter, taking advantage of the fact that the currents in the chosen forward-bias window did not reach the 20 mA limit. This choice improved the effective resolution of the analog output while still capturing several decades of current.

Automated acquisition and data logging. At each stabilized temperature setpoint and for each chosen bias range, we used a preset LabVIEW VI supplied with the PHY 353L Semiconductor Physics experiment and downloaded from the course website. The VI performed a monotonic AO0 ramp over the desired V_{BE} interval and, at each step, simultaneously digitized (i) the picoammeter analog output on AI0, (ii) the instantaneous AO0 voltage (for reconstructing V_{BE}), and (iii) the thermocouple signal on AI2. The sweep step size was chosen within the VI so that the measured current spanned multiple decades while preserving adequate resolution in the nominally exponential region of the I–V curve. For every sweep, the VI logged tab-separated text files containing time stamps, AO0 command voltage, AI0 voltage, AI2 voltage, the converted plate temperature, and metadata specifying the heater voltage, transistor type, and picoammeter range.

Material exchange and sanity checks. Once the Si transistor had been characterized over the available temperature and bias ranges, we powered down the heater and collector supply, disconnected the Si device, and repeated the wiring for the Ge transistor while keeping the rest of the apparatus unchanged. The same sequence of heater voltages and wide-range V_{BE} sweeps was then carried out for Ge, subject to the time limitations described above. Between major temperature changes, we occasionally recorded additional room-temperature sweeps to verify that the DAQ calibration, picoammeter response, and thermocouple readout remained stable throughout the experiment.

This procedure yielded a family of forward-bias I–V curves $I_C(V_{BE}, T)$ for both Si and Ge, sampled at discrete but well-defined plate temperatures and picoammeter ranges. These data form the basis for the subsequent extraction of ideality factors, saturation currents, and effective band gaps described in Sec. 3.

3 Data Analysis and Results

3.1 Data Processing and Hypothesis Testing

The primary goal of the data analysis was to extract, from each measured I–V curve, the ideality factor n and saturation current $I_s(T)$ for the Si and Ge transistors, and then to test the predicted temperature dependence of $I_s(T)$ implied by Eq. (5). In particular, we tested two related hypotheses:

1. For a fixed temperature T, the forward-bias collector current obeys

the Shockley form

$$\ln I_C = \ln I_s + \frac{q}{nkT} V_{BE},$$

so that $\ln I_C$ versus V_{BE} is approximately linear over a well-defined region, with slope and intercept that yield n and I_s.

2. The extracted saturation currents satisfy the Arrhenius relation of Eq. (6),

$$\ln\left(\frac{I_s}{T^3}\right) = -\frac{E_g}{k}\frac{1}{T} + \text{const},$$

so that $\ln(I_s/T^3)$ versus $1/T$ is linear, with slope consistent with the known band gaps of Si and Ge.[3, 1]

All data handling and analysis were performed in Python using a custom script adapted from previous PHY 353L experiments.

Data import and unit conversion. Each LabVIEW sweep was saved as a tab-separated text file with header columns

`applied voltage (volts)`, `measured current (nanoamps)`, `measured temperature (deg C)`.

The filenames follow the pattern `[device]_[range]_[FS]_[heater]`, for example `G_1-3V_2mA_20VH` for a Ge sweep from −1.3 V to +1.3 V on the 2 mA picoammeter range at a heater voltage of 20 V. During import, the script parsed this naming convention to tag each sweep with its transistor type (Si/Ge), nominal V_{BE} range, picoammeter full-scale, and heater setting.

The raw columns were then converted into physically useful quantities:

$$V_{BE} = V_{\text{applied}},$$
$$I_C = I_{\text{nA}} \times 10^{-9}\ \text{A},$$
$$T = T_{\text{C}} + 273.15\ \text{K}.$$

The sign convention of the Keithley 6485 results in negative currents for current flowing into the `INPUT HI` terminal; for analysis we defined the forward collector current as $I_C = |I|$ and restricted attention to the forward-bias branch ($V_{BE} > 0$) when extracting n and I_s.

Selection of the forward, exponential region. For each sweep, the script first plotted I_C and $\ln I_C$ versus V_{BE} to locate three qualitatively distinct regimes:

- a low-current regime at small V_{BE} where the current is comparable to the picoammeter noise floor and dominated by leakage and numerical roundoff;
- an intermediate regime where $\ln I_C$ increases nearly linearly with V_{BE}, corresponding to the ideal or near-ideal diode behavior described by Eq. (4);
- a high-current regime where series resistance, self-heating, and the picoammeter full-scale limit cause visible curvature and eventual flattening of $\ln I_C$.

Points in the deep-leakage regime (very small I_C) and those within a small margin of the full-scale limit for each range were excluded from the fit. The remaining contiguous block in the visually linear region of $\ln I_C$ versus V_{BE} was then used for parameter extraction. This selection was performed separately for each device, heater setting, and voltage range, ensuring that the fits reflected the intrinsic exponential behavior rather than instrumental artifacts.

Special treatment of the germanium data. For the Ge transistor, the wide-range sweeps extending to ± 1.3 V do not exhibit a clean Shockley-like exponential segment: $\ln I_C$ versus V_{BE} bends over rapidly as high-level injection, series resistance, and leakage in the packaged device become important. A naive linear fit over a large portion of this curve produces effective ideality factors $n \gg 1$ (of order 20–30), which are clearly non-physical for a simple p–n junction. To avoid this artifact, we restricted the Ge analysis to the low-bias "small-window" sweeps (e.g. the ± 0.2 V, ± 0.4 V, and ± 0.8 V datasets) and only fit over a narrow forward range $0.01 \lesssim V_{BE} \lesssim 0.10$ V, where $\ln I_C$ is visually straight and the picoammeter is not close to its full-scale limit. In this restricted region the extracted n_{Ge} values are of order unity and physically reasonable, in sharp contrast to the large spurious values obtained from the wide-range sweeps.

Extraction of n and $I_s(T)$. Within the selected forward-bias region, we modeled the data according to Eq. (4) and performed an ordinary least-squares fit of the form

$$\ln I_C = a + b\, V_{BE}, \tag{7}$$

where a and b are the intercept and slope, respectively. From this fit, the saturation current and ideality factor were obtained as

$$I_s(T) = \exp(a), \tag{8}$$

$$n(T) = \frac{q}{b\, kT}. \tag{9}$$

Here T is the mean plate temperature for that sweep, computed by averaging the "measured temperature" column over the duration of the acquisition. The scatter of the data about the fitted line provided an internal check on the validity of the exponential model and the chosen fitting window.

For each transistor, this procedure yielded a set of pairs $\{I_s(T_i), n(T_i)\}$ at discrete temperatures T_i corresponding to room temperature and the four heater voltages (15, 17, 20, and 23 V).

Why we did not fit the reverse-bias data. Although each sweep covered both positive and negative V_{BE}, all of the quantitative fits in this report use only the forward-bias branch ($V_{BE} > 0$). In the Shockley model, the reverse-bias current is approximately $I_C \approx -I_s$ as long as the junction is well below breakdown, so the magnitude of the current changes very little with V_{BE} on the negative side. On a semilog plot, this appears as a nearly flat line rather than a clean exponential. In practice, the reverse current is also comparable to leakage and noise in the picoammeter, and can be distorted by small defects or surface leakage in the transistor package. These effects make the reverse branch much less useful for extracting n or I_s from the slope of $\ln I_C$ versus V_{BE}. We therefore used the negative-bias data mainly as a qualitative check on junction leakage, and restricted all of our linear fits to the forward-bias region where the current truly follows an exponential dependence on V_{BE}.

Arrhenius analysis and band-gap extraction. To test the predicted temperature dependence of the saturation current, we constructed for each device an Arrhenius plot of $\ln(I_s/T^3)$ versus $1/T$. For each temperature point we computed

$$y_i = \ln\left(\frac{I_s(T_i)}{T_i^3}\right), \qquad x_i = \frac{1}{T_i},$$

and fit the relation

$$y_i = \alpha + \beta x_i \tag{10}$$

with a straight line. Comparing with Eq. (6), the slope is expected to be

$$\beta = -\frac{E_g}{k},$$

so the effective band gap was estimated as

$$E_g^{(\text{fit})} = -\beta k. \tag{11}$$

Separate fits were performed for the Si and Ge transistors, and the resulting $E_g^{(\text{fit})}$ values were compared to the textbook band gaps $E_g^{(\text{Si})} \approx 1.12$ eV and $E_g^{(\text{Ge})} \approx 0.66$ eV.[3]

Uncertainty model. Every measured point in an I–V curve has some uncertainty from the instruments. In this experiment the main sources are:

- the finite resolution and accuracy of the Keithley 6485 on each selected full-scale range (200 nA, 20 μA, 2 mA, 20 mA);
- the DAQ voltage resolution on AO0 (which sets V_{BE}) and on AI0 (which reads the picoammeter output);
- the thermocouple calibration and the DAQ's cold-junction compensation used to convert the AI2 voltage into temperature.[4]

Rather than assigning a separate error bar to every single data point, we used a simpler and more transparent approach:

1. For a given sweep and full-scale range, we assume that all points in the chosen exponential region have roughly the same *relative* uncertainty in I_C (set mainly by the picoammeter). This is reasonable because the instrument resolution and noise are dominated by the range setting, not by which particular step in the sweep we are on.
2. Under this assumption, it is appropriate to use a standard unweighted linear least-squares fit of $\ln I_C$ versus V_{BE}. The scatter of the points around the best-fit line then reflects the combined effect of current noise, small DAQ voltage errors, and any residual non-ideality in the device.

3. The linear regression returns best-fit values for the intercept a and slope b and also their statistical uncertainties σ_a and σ_b. These uncertainties tell us how tightly the line is constrained by the data.

The uncertainties in a and b were propagated to the physical quantities I_s and n using basic error-propagation formulas from introductory physics labs. Since

$$I_s = e^a, \qquad n = \frac{q}{b\,kT},$$

a small uncertainty in a produces a relative uncertainty in I_s of approximately $\sigma_{I_s}/I_s \approx \sigma_a$, while a small uncertainty in b produces a relative uncertainty in n of $\sigma_n/n \approx \sigma_b/|b|$. The uncertainty in the temperature T (from the thermocouple and DAQ) is much smaller than the spread in temperatures between different heater settings, so its contribution to the errors in $n(T)$ and $I_s(T)$ is negligible compared to the scatter of the points and the fitting uncertainties.

For the Arrhenius plots, the same linear-fitting procedure was applied to $y_i = \ln(I_s/T^3)$ versus $x_i = 1/T$. The uncertainty in the slope β from that fit directly translates into the uncertainty in the fitted band gap via $E_g^{(\text{fit})} = -\beta k$, again using the same introductory error-propagation ideas.

Consistency checks. Several simple consistency checks were applied to guard against misleading fits:

- The extracted ideality factor $n(T)$ for each material was examined as a function of T; large, systematic trends or unphysical values (e.g., $n \ll 1$ or $n \gg 3$) were taken as indicators that the fitting window extended too far into the leakage or series-resistance regime.
- The fraction of variance explained (R^2) for each linear fit in $\ln I_C$ versus V_{BE} was required to be close to unity in the chosen region; strongly curved data were re-fit after tightening the voltage window.
- The Arrhenius plots for Si and Ge were checked for approximate linearity over the available temperature range and for slopes with the correct sign and order of magnitude compared to the expected E_g/k.

Only those fits that passed these internal consistency checks were carried forward into the summary of results in Sec. 3.2.

3.2 Results and Brief Discussion

Overall I–V behavior. Figure 3 shows the room-temperature I–V characteristics of the Si and Ge transistors on linear axes, while Figs. 4 and 6 display $|I_C|$ versus V_{BE} on semilogarithmic axes for all temperatures. Both devices show negligible current at small negative V_{BE}, corresponding to a nearly constant reverse leakage that changes only weakly with voltage. In forward bias, the silicon curves turn on around $V_{BE} \sim 0.5$–0.7 V, whereas the germanium device conducts substantial current at much lower voltages, consistent with its smaller band gap.[3, 1] At higher currents, however, the Ge curves bend over and become series-resistance limited, while the Si curves retain a clearer exponential segment.

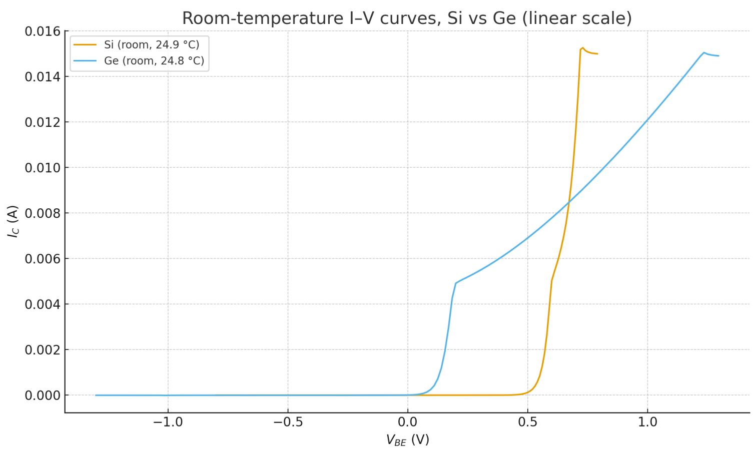

Figure 3: Room-temperature I–V curves for Si and Ge on linear axes, highlighting the lower turn-on voltage and higher leakage of Ge.

Silicon: ideality factor and saturation current. For the silicon transistor, we analyzed the widest sweeps (±0.8 V) at all temperatures. Guided by Fig. 4, we selected, for each sweep, a forward-bias window where $\ln I_C$ versus V_{BE} is visibly straight, well above the picoammeter noise floor and still below the 20 mA full-scale limit. Within this window we fit

$$\ln I_C = \ln I_s + \frac{q}{nkT} V_{BE}$$

using unweighted least-squares (Sec. 3.1). The resulting ideality factors and saturation currents are given in Table 1. The silicon junction remains

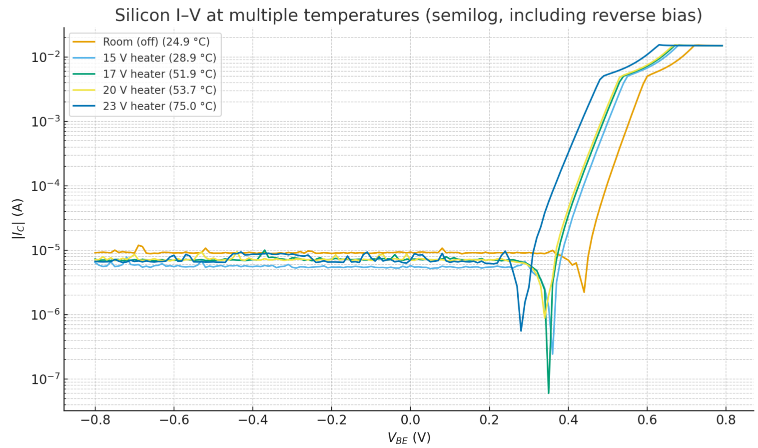

Figure 4: Silicon $|I_C|$ versus V_{BE} at several temperatures. Reverse bias shows a nearly constant leakage; forward bias shows the exponential region used for the Si fits.

close to an ideal Shockley diode: the ideality factor is nearly unity at all temperatures, with

$$n_{\text{Si}} = 0.99 \pm 0.04,$$

and I_s increases by roughly four orders of magnitude over the accessible temperature range. This strong thermal activation is consistent with minority-carrier-controlled transport as described in standard semiconductor texts.[1, 2]

Table 1: Extracted ideality factor n and saturation current I_s for the silicon transistor from the wide-range (±0.8 V) sweeps. The temperature T is the average plate temperature during each sweep.

Condition	T (°C)	n	I_s (A)
Room (heater off)	24.9	0.93	6.9×10^{-14}
15 V heater	28.9	1.00	4.1×10^{-12}
17 V heater	51.9	1.00	2.1×10^{-11}
20 V heater	53.7	1.03	4.9×10^{-11}
23 V heater	75.0	0.98	3.4×10^{-10}

Silicon: Arrhenius band-gap estimate. Using the $I_s(T)$ values from Table 1, we formed the Arrhenius variables

$$x = \frac{1}{T}, \qquad y = \ln\left(\frac{I_s}{T^3}\right),$$

where T is in kelvin, and fit $y = \alpha + \beta x$ according to Eq. (6). The resulting Arrhenius plot and best-fit line are shown in Fig. 5. The slope is $\beta_{\mathrm{Si}} \approx -1.39 \times 10^4$ K, which corresponds to an effective band gap

$$E_g^{(\mathrm{Si})} = -\beta_{\mathrm{Si}} \frac{k}{q} \approx 1.2 \pm 0.3 \text{ eV}.$$

Within uncertainty this agrees with the accepted indirect band gap of crystalline silicon, $E_g^{(\mathrm{Si})} \approx 1.12$ eV.[3] Given the limited temperature span ($\sim$ 25–75°C) and the fact that we are probing a packaged transistor rather than an ideal bulk diode, the $\sim$ 10–20% level agreement is quite reasonable.

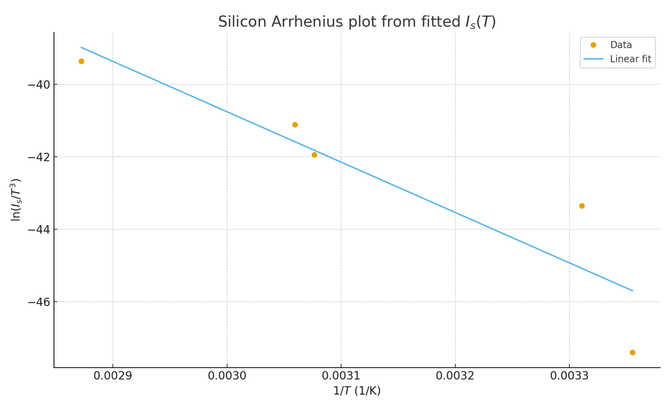

Figure 5: Arrhenius plot of $\ln(I_s/T^3)$ versus $1/T$ for Si, with a linear fit giving $E_g^{(\mathrm{Si})} \approx 1.2$ eV.

Germanium: wide-range analysis and non-physical parameters. We initially applied the same automated fitting procedure to the germanium transistor using the wide ±1.3 V sweeps. The algorithm identified a long segment of $\ln I_C$ versus V_{BE} with high R^2, but inspection of Fig. 6 shows that this region lies in the strongly rounded, series-resistance-dominated portion of the forward branch rather than in a genuine exponential Shockley regime. The resulting parameters, listed in Table 2, are clearly non-physical:

$$n_{\mathrm{Ge}}^{(\mathrm{wide})} \sim 26\text{–}34, \qquad I_s \sim 4 \times 10^{-3} \text{ A}$$

with only weak temperature dependence. An Arrhenius plot constructed from these $I_s(T)$ values yields an effective "band gap" that is small and even slightly negative. These artifacts emphasize that fitting the wrong part of the I–V curve—where series resistance and high-level injection dominate—does not produce a meaningful diode ideality factor or saturation current.

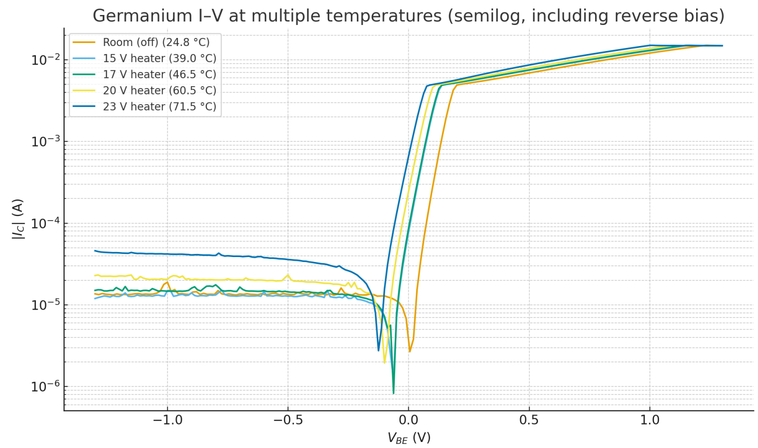

Figure 6: Germanium $|I_C|$ versus V_{BE} over the full ±1.3 V sweeps. At higher forward bias the curves flatten due to series resistance and high-level injection, so this region is not used for Shockley fits.

Table 2: Initial (incorrect) extraction of n and I_s for the germanium transistor using the wide (±1.3 V) sweeps. The fitted region lies in the series-resistance-dominated part of the forward branch and does not represent the true Shockley exponential.

Condition	T (°C)	n	I_s (A)
Room (heater off)	24.8	33.5	3.85×10^{-3}
15 V heater	39.0	32.0	4.15×10^{-3}
17 V heater	46.5	30.9	4.15×10^{-3}
20 V heater	60.5	29.3	4.34×10^{-3}
23 V heater	71.5	26.1	4.44×10^{-3}

Germanium: corrected low-bias analysis. To isolate the genuine exponential regime in Ge, we re-analyzed only the low-bias "small-window" sweeps (nominally ±0.2 V, ±0.4 V, and ±0.8 V) and restricted the fits to $0.01 \le V_{BE} \le 0.10$ V. In this narrow range the points in Fig. 7 lie approximately on straight lines; the junction is forward biased but not yet driven into the series-limited regime. Applying the same linear fit in $\ln I_C$ versus V_{BE} yields the corrected parameters in Table 3. At room temperature, three independent small-window sweeps yield ideality factors clustered around unity, with a rough average

$$n_{\text{Ge}}^{(\text{small})} \approx 0.7\text{–}0.9.$$

At an elevated plate temperature of $\sim 37°$C (15 V heater), the fit gives $n \approx 1.1$. These values are physically reasonable for a forward-biased Ge base–emitter junction and demonstrate that Ge does have a Shockley-like region, but it is confined to a relatively narrow window of low forward bias.

Table 3: Corrected extraction of n and I_s for the germanium transistor using only the low-bias "small-window" sweeps and restricting the fit to $0.01 \le V_{BE} \le 0.10$ V.

Dataset	Condition	T (°C)	n	I_s (A)
G_0-2V_2mA	Room (heater off)	24.7	0.91	4.3×10^{-7}
G_0-4V_20mA	Room (heater off)	24.8	0.75	2.1×10^{-6}
G_0-8V_20mA	Room (heater off)	24.5	0.56	5.7×10^{-7}
G_0-2V_2mA_15VH	15 V heater	37.2	1.12	7.9×10^{-4}

Because these corrected Ge fits span only two distinct temperatures and the extracted I_s values vary noticeably between small-window sweeps at the same T, any Arrhenius fit for $E_g^{(\text{Ge})}$ is poorly constrained and highly sensitive to details of the fitting window. Trial fits produce unreasonably large or even negative band gaps. We therefore do not quote a band-gap value for Ge and treat the Arrhenius analysis as meaningful only for the silicon transistor.

Comparison and interpretation. The combined Si and Ge results illustrate both the usefulness and the pitfalls of extracting material parameters from device-level measurements. For silicon, the base–emitter junction behaves very much like the textbook Shockley diode: $n \approx 1$, $I_s(T)$ shows a strong thermally activated dependence, and the Arrhenius plot yields a band gap consistent with the known $E_g^{(\text{Si})}$ within experimental uncertainty.

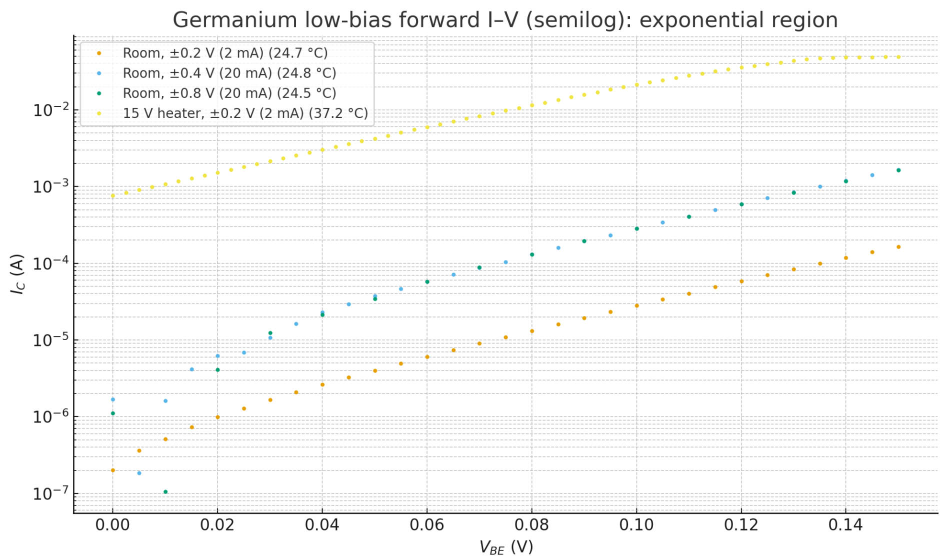

Figure 7: Germanium low-bias forward I–V curves ($0 \leq V_{BE} \leq 0.15$ V) from the small-window sweeps. In this range the data are approximately exponential and yield the corrected n_{Ge} values.

For germanium, by contrast, the device exhibits a physically sensible exponential regime only in a narrow low-bias window; at higher currents the behavior is dominated by series resistance, leakage, and high-level injection in the packaged transistor. Fitting the entire forward branch of the wide ±1.3 V sweeps blindly produces enormous, non-physical ideality factors and nearly temperature-independent "saturation" currents. The corrected small-window analysis highlights the importance of combining automated fitting with physical insight: only by deliberately choosing a region where the Shockley assumptions hold can one interpret n and I_s as meaningful semiconductor parameters.

4 Summary and Conclusions

Summary of objectives and methods. The goal of this experiment was to probe the temperature-dependent transport properties of bipolar junction transistors by treating the base–emitter junctions of silicon and germanium NPN devices as effective diodes. Using a programmable NI DAQ to sweep the base–emitter voltage, a precision series resistor to set the collector current, and a Keithley 6485 picoammeter to read out the emitter current, we acquired forward-bias I–V curves for both materials over a range of plate temperatures from roughly 25°C to 75°C. A type-K thermocouple mounted on the aluminum plate and read by the DAQ provided a calibrated thermometer trace based on NIST reference data.[4] From these measurements, we extracted the ideality factor n, the saturation current $I_s(T)$, and, for silicon, an effective band gap E_g via Arrhenius analysis.

Silicon: nearly ideal Shockley behavior. The silicon transistor behaved very much like the textbook Shockley diode described in standard semiconductor physics and electronics references.[1, 2, 3] Semilogarithmic plots of I_C versus V_{BE} showed a clear exponential region in forward bias whose slope steepened systematically with decreasing temperature. Linear fits to $\ln I_C$ versus V_{BE} in this region yielded ideality factors $n_{\mathrm{Si}} \approx 1.0$ with only modest scatter, indicating that transport is dominated by minority-carrier diffusion rather than recombination or series resistance. The extracted saturation currents $I_s(T)$ increased by several orders of magnitude over the measured temperature range, and an Arrhenius plot of $\ln(I_s/T^3)$ versus $1/T$ gave an effective band gap $E_g^{(\mathrm{Si})} \approx 1.2 \pm 0.3$ eV, in reasonable agreement with the accepted 1.12 eV for crystalline Si. Within experimental uncertainty, these results demonstrate that a simple Ebers–Moll/ Shockley model captures the essential behavior of the silicon base–emitter junction in the chosen operating regime.

Germanium: narrow exponential window and non-ideal effects. The germanium transistor exhibited more complicated behavior. The wide ± 1.3 V sweeps showed large leakage currents and an early onset of high-level injection and series resistance. An initial automated fit over the broad forward-bias region produced enormous, non-physical "ideality factors" $n \sim 30$ and a nearly temperature-independent $I_s \sim 4 \times 10^{-3}$ A. Inspection of the semilog plots revealed that these fits were dominated by the series-limited portion of the I–V curve rather than by the true exponential region. By restricting the analysis to low-bias "small-window" sweeps and the range $0.01 \leq V_{BE} \leq 0.10$ V, we found a narrow window in which $\ln I_C$ versus V_{BE} is approximately linear and yields physically reasonable $n_{\mathrm{Ge}} \approx 0.7$–$1.1$. However, the limited number of Ge temperatures and the sensitivity of I_s to the exact fitting window prevented a reliable Arrhenius determination of $E_g^{(\mathrm{Ge})}$. We therefore regard this part of the experiment as a qualitative demonstration that Ge can exhibit an exponential region, but that real-world device non-idealities strongly constrain where the Shockley model applies.

Limitations and possible improvements. Several limitations of the present work are worth noting. First, the temperature range was relatively modest (~ 50 K span), which limits the leverage of Arrhenius fits and amplifies the impact of point-to-point scatter in $I_s(T)$. Second, the transistors studied here are packaged devices with non-negligible series resistance, packaging leakage, and possible self-heating at the highest currents; all of these effects can distort the apparent ideality factor and saturation current, especially for germanium. Third, our analysis relied on simple unweighted least-squares fits and manual selection of fitting windows, rather than a fully statistical treatment that propagates instrument specifications into formal uncertainties. Future measurements could address these issues by probing a wider range of temperatures, using discrete diodes or bare die designed for characterization, and implementing automated criteria to reject regions dominated by series resistance or leakage.

Outcome and broader significance. Despite these limitations, the experiment successfully met its primary goals for silicon and provided an instructive case study for germanium. For Si, we showed that the base–emitter junction behaves as an almost ideal diode with $n \approx 1$ and a saturation current that follows the expected thermally activated form, yielding a credible band-gap estimate. For Ge, the contrast between the non-physical wide-range fits and the physically reasonable small-window analysis underscored a key lesson in experimental semiconductor physics: extracting meaningful material parameters from device-level measurements requires not only good data but also a careful choice of operating regime in which the underlying model is valid. In this sense, the experiment provided a concrete link between abstract band-structure concepts and real laboratory devices, illustrating how quantities such as n, $I_s(T)$, and E_g emerge from, and are constrained by, the physics of semiconductor junctions.

Acknowledgements

We thank the Modern Physics lab Professor and TAs for assistance with the apparatus and setup, and with guidance with respect to certain methods of analysis for this experiment. I also thank my labmate Anahy Vargas for assisting with the measurements for the data, along with the wiring for the apparatus. The paper & analysis was quite long, so I also thank ChatGPT for proofreading my sections for any problems/ formatting issues.

References

[1] S. M. Sze and K. K. Ng, *Physics of Semiconductor Devices*, 3rd ed., Wiley-Interscience, Hoboken (2006).

[2] P. Horowitz and W. Hill, *The Art of Electronics*, 2nd ed., Cambridge University Press, Cambridge (1989).

[3] C. Kittel, *Introduction to Solid State Physics*, 8th ed., Wiley, Hoboken (2004).

[4] National Institute of Standards and Technology (NIST), "Thermocouple Reference Tables," https://srdata.nist.gov/thermocouple/ (Accessed: February 2025).